J. Astrophys. Astr. (1980) **1**, 129–154

Central Regions of Sérsic-Pastoriza Galaxies: A Photographic Study

T. P. Prabhu *Indian Institute of Astrophysics, Bangalore 560034*

Received 1980 August 6; accepted 1980 October 24

Abstract. A classification scheme is proposed for the central regions of Sérsic-Pastoriza galaxies based on high resolution photographs of 50 objects in the integrated light (4000 Å–8700 Å). Structures of two different linear scales are recognized: (1) nucleus ($\lesssim$1 kpc) and (2) perinuclear formation ($\sim$1·5 kpc). The perinuclear formation is weak in class κ while the nucleus is too faint to detect in class ι. In the intermediate classes ϵ and σ both the components are bright. Class ϵ has an elliptical perinuclear formation with little gas while the class σ consists of bright H II complexes and dust. Observations of a few galaxies in the infrared and the blue ends of the image tube response show that the nucleus is generally redder than its surroundings. Equal intensity contours and the luminosity profiles are presented for the central regions of 27 galaxies. A comparison of their axial ratios with those of the parent galaxies indicates that the perinuclear formations are prolate or barlike. The dependence of the peak surface brightness of the central formation on the size of the bar is investigated as also the dependence of the central surface brightness of the bar on the size of the bar. The following major conclusions are drawn:

(1) The peak central surface brightness of the perinuclear formation varies as the square of the bar length. This relation implies that the bar induces the infall of gas from the bar-disk region.

(2) The formations of class σ move towards class ϵ as star formation ceases and the massive stars die.

(3) The class ι differs from class σ in the intensity of the burst of star formation. Low luminosity of the parent galaxies in class ι implies less infall of gas and higher domination of the bar potential on the perinuclear formation. Thus the class ι structures are more prolate than those of class σ.

(4) The central brightness of the bars varies directly as the length of the bar.

Key words: galaxies—central regions—bursts of star formation—surface photometry

1. Introduction

Morgan (1958) noticed that the central regions of some spiral galaxies consist of clusters of bright spots which he termed ' nuclear hot spots '. Early spectroscopic work showed that the hot spots are mere complexes of H II regions (Burbidge and Burbidge 1960, 1968). A wealth of spectroscopic information has been accumulated in recent years (Osmer, Smith and Weedman 1974; Oka *et al.* 1974; Pastoriza 1975; Turnrose 1976; Alloin and Kunth 1979; Wakamatsu and Nishida 1980). One concludes from these data that the central regions of some spiral galaxies have recently received a fresh supply of gas and a burst of star formation has been triggered.

Sérsic and Pastoriza (1965) and Sérsic (1973) have systematized and enlarged upon Morgan's list. Their criterion of ' peculiar nucleus ' is ' a change in the slope of luminosity profile and evidence of some structure ' (Sérsic 1973). This definition is broader than Morgan's and hence includes in addition to the conventional hot-spot systems, the ' amorphous nuclei ' or ' spherical formations surrounded by diffuse asymmetric structure '. Though not complete to any given magnitude limit, nor to any part of the sky, Sérsic's finding list has the advantage of selection of central regions of spiral galaxies based on a unique criterion. It is hence unfortunate that despite the coinage of the term ' Sérsic-Pastoriza (S-P) galaxies' (Osmer, Smith and Weedman 1974) the central regions generally studied are only the hot-spot subclass of Sérsic's list. A closer examination of a larger number of S-P galaxies and an enlargement of Sérsic's finding list is urged by the following information on the central regions of spiral galaxies:

(1) Sérsic's criterion of ' a change in the luminosity profile ' compares well with the ' nucleus-shoulder-arms ' structure of Seyfert galaxies (Morgan, Walborn and Tapscott 1971).

(2) Intense emission lines are quite common in the hot-spot galaxies and differ from the spectra of Seyfert galaxies mainly in their breadth. Véron *et al.* (1979, 1980) and Véron, Véron and Zuiderwijk (1980) have seen faint broad components in the emission line profiles of several ' emission line galaxies ' and suspect that a Seyfert nucleus may at times be hidden within a giant H II region.

(3) Large infrared (10 μm) excess is observed in the central regions of several hot-spot galaxies: NGC 2903, 3627, 4258, 4303, 5236 (Rieke and Lebofsky 1978); 3504, 4051 (Rieke and Low 1972); 4064 (Kleinmann and Low 1970); and 7552 (Kleinmann and Wright 1974). The near infrared observations of NGC 1365 and 1808 by Glass (1976) also show excess over the stellar radiation. The excess is interpreted to be due to the reemission by dust heated by the radiation from H II complexes (Telesco and Harper 1980). The amount of the excess is midway between the excess in Seyfert nuclei and in the Galactic nucleus. Some S-P galaxies exhibit an activity of such an intermediate degree in X-rays: NGC 1097 (Ku *et al.* 1979), 1365 (Ward *et al.* 1978) and 1672 (Griffiths, Feigelson and van Speybroeck 1979) are examples of this category. Weak compact central radio sources similar to the ones contained in Seyfert galaxies are found by van der Kruit (1973) in several S-P galaxies (NGC 1300, 2903, 3310, 4258, 4321 and 5383). Two S-P galaxies, NGC 4051 and 4151 are also Seyferts and exhibit the above characteristics.

Our aim to investigate a sample of 50 S-P galaxies (Section 2) has been

(a) to recognize and establish a class of events in the central regions of S-P galaxies,

(b) to arrive at a morphological classification scheme which may provide clues to the strength of and the evolutionary stage of the event (Section 3) and

(c) to investigate the photometric parameters of the central substructure and to search for the clues to the mechanism of the infall of gas.

The observational data are presented in the form of equal intensity contours and equivalent luminosity profiles in Section 4. The distribution of colours using a wide base line (blue and image tube infrared) has been presented for six of the programme galaxies in Section 5. The geometrical and the photometric parameters of the sample are discussed in Section 6 followed by a summary of the results.

2. Observations

We have photographed the central regions of 50 S-P galaxies at the f/13 Cassegrain focus of the 102-cm reflector telescope at the Kavalur Observatory. A Varo 8605 image tube with an S-20 photocathode was employed in a cathode-grounded configuration. The image tube has a P-20 phosphor and input and output face plates of fiber optics. The image scale in the central region of the image tube is 15·5 arcsec mm^{-1}. Kodak IIa-D plates were used in contact with the output face plate. The resolution of the image tube and also of the photographic emulsion is 60 lp mm^{-1} which corresponds to 0·24 arcsec at the image scale mentioned above. Thus the final resolution is limited only by the astronomical seeing which was close to one arcsec on an average. The large image scale results in several instrumental resolution elements per seeing disc ($\sim$17 on an average) and hence considerably improves the signal-to-noise ratio.

The response of the image tube extends from 4000 Å (fiber optics cut-on) to 8700 Å A blue region (4000 Å–4600 Å) was isolated employing 2 mm of Schott BG12 filter while a Wratten 89B filter enabled the isolation of an infrared region (7000 Å–8700 Å). Six of the programme galaxies were observed in both these bands. The star-like nucleus and the stellar population of the substructure surrounding the nucleus are visible better in the infrared than in the blue. The hot spots are on the other hand seen more distinctly in the blue. All the 50 programme galaxies were photographed in the integrated light of 4000 Å–8700 Å; they represent the nucleus, the stellar population and also the hot spots.

The exposure times ranged from 1 to 10 minutes in integrated light, 5 to 20 minutes in the blue band and 3 to 15 minutes in the infrared. Several graded exposures were obtained (3 in the majority of cases). The thermal background of the image tube was negligible in all the observations. The sky background was also very low except on the longest exposures. The radial and azimuthal variations in the sensitivity of the image tube, as also the pin cushion distortion have not introduced significant variation over the small sizes of interest ($\lesssim$ 4 mm). The images were geometrically centred well near the maximum of tube sensitivity. Different exposures were obtained by shifting the position of the image slightly. Whenever the chicken-mesh due to fiber optics was superposed on the images, plates were discarded. The instances were rare since the contrast of the chicken-mesh was generally very low.

Calibration to relative intensities was achieved by photographing the spectrum of a

tungsten lamp through a rotating sector on a separate piece of the same photographic plate as was used for the exposure of the galaxy. The image tube was not employed in this exposure and its response to intensity was assumed to be linear.

3. Classification

The seeing-limited photographs obtained by us reveal two distinct components in the central regions of S-P galaxies:

(a) Nucleus: A bright unresolved or barely resolved formation of $\lesssim 4$ arcsec extent. It is generally redder than the surrounding region.

(b) Perinuclear formation: A substructure of 10–30 arcsec radius around the nucleus.

The relative brightness of these two subsystems varies from one galaxy to another. We propose here a classification scheme for S-P galaxies in which we distinguish between different types according to the relative brightness of the nuclear and the perinuclear region. The central regions with bright nucleus and a very faint perinuclear region are classified as type κ, while those with a very faint nucleus and a bright perinuclear region are classified as type ι. The central regions that show both the components are assigned intermediate classes according to the morphological appearance of the perinuclear formation. A high degree of concentration is assumed to be an indication of the presence of the nucleus even when the latter is not clearly discernible. The classification criteria are listed in Table 1. The central formations of typical members of the major classes (κ, ϵ, σ, ι) are shown in Fig. 1. The class $\epsilon\sigma$ is of intermediate nature between the classes ϵ and σ and $\sigma\iota$ between σ and ι. This classification of 50 S-P galaxies is presented in Table 3 in Section 6.

The above classification scheme was induced by the great degree of regularity noticed in the structure of the perinuclear formations. The hot-spots are generally contained within a region that appears elliptical or oval in class σ and generally follow the pattern of a pseudo-ring formed by two tight spiral arms. The sense of opening can often be traced to be similar to that of the main spiral arms of the galaxy. The hot spots in class ι are aligned in a straight line, and are contained within a barlike region. The perinuclear formations of class ϵ are elliptical or oval structures with smooth distribution of intensity. Morphologically there is a great resemblance

Table 1. Morphological classification scheme for the central regions of Sérsic-Pastoriza galaxies.

Class	Nucleus	Perinuclear formation
κ	very bright	very faint or absent
ϵ	bright	bright with elliptical boundary and smooth intensity distribution
$\epsilon\sigma$	bright	bright smooth intensity distribution without a well-defined boundary
σ	bright	bright, distinct or fairly distinct hot spots; a spiral pattern is often evident in dark lanes, hot spots, or in underlying red population
$\sigma\iota$	faint	barlike, generally resolved into hot spots
ι	very faint or absent	barlike formation of faint hot spots

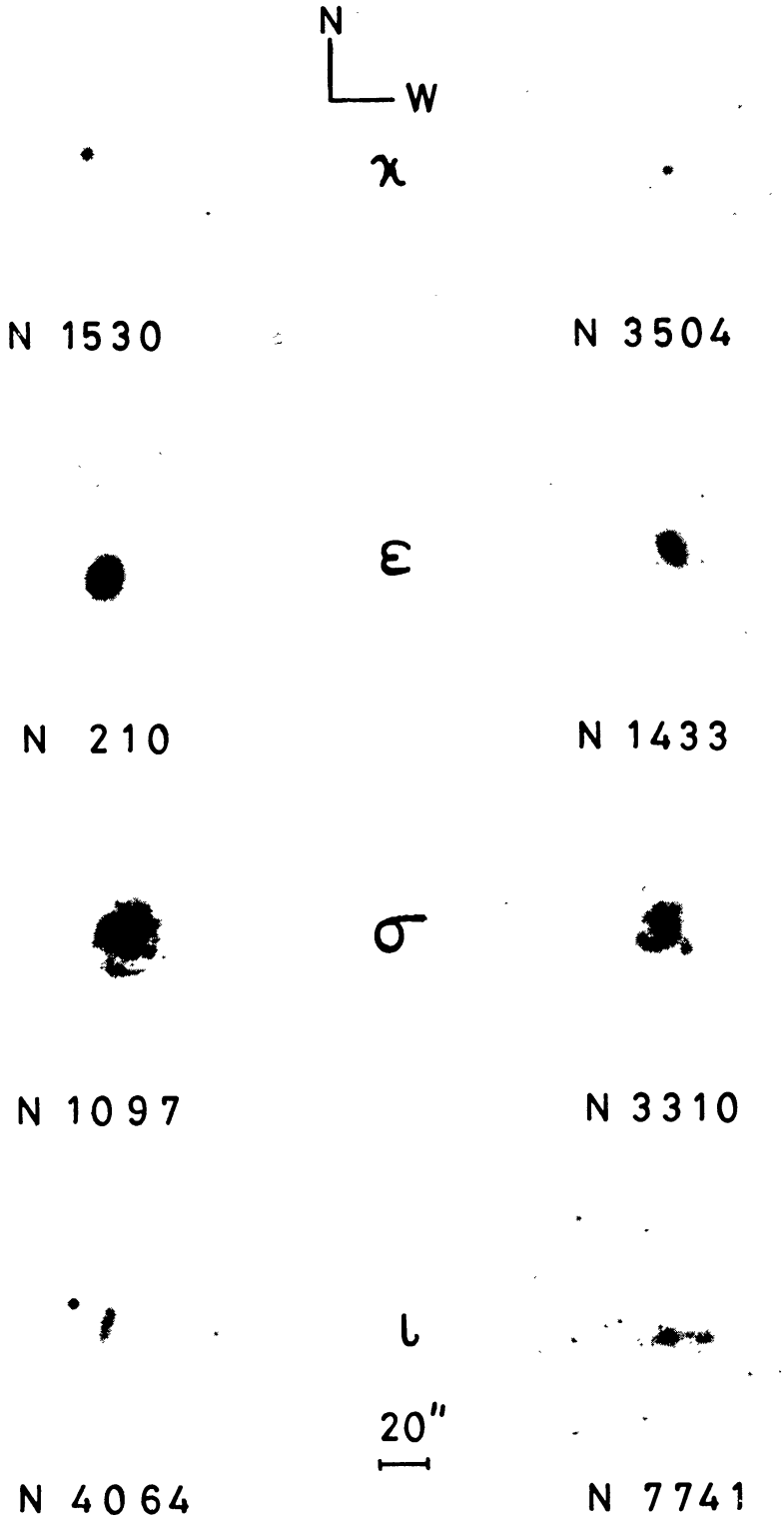

Figure 1. Contrast prints of the central regions of typical members of the major classes of S-P galaxies. The orientation and the scale are the same for all the galaxies.

between our classification scheme for perinuclear regions and the Hubble scheme for galaxies. We have hence drawn the nomenclature from this similarity: ϵ for elliptical, σ for spiral, ι for irregular. Our class κ resembles Zwicky's red compact galaxies.

Sérsic (1973) classified the central regions into two types: (1) HS: Structures with distinct hot spots, and (2) AN: ' amorphous nuclei or spherical formations surrounded by diffuse asymmetric structure '. He also included the dumb-bell like formation (dB) of NGC 1087 and NGC 1140 as a variant of AN. We classify these two objects as $\sigma\iota$ since they appear to contain two faint hot spots. This classification is however not very certain. Among the 50 galaxies classified by us, Sérsic (1973) has classified 41 as AN or HS and two as dB. The galaxies NGC 1415 and NGC 1433 are both classified as AN by Sérsic and Pastoriza (1965). We show in Fig. 2 the fraction of galaxies of Sérsic types AN or HS in each of our class. The dB galaxies are excluded. A high degree of correlation is seen in the sense that the AN contains mostly the earlier classes (ϵ) while the HS contains the later ones (σ, ι). Thus our classification scheme is only an enlargement of Sérsic's scheme.

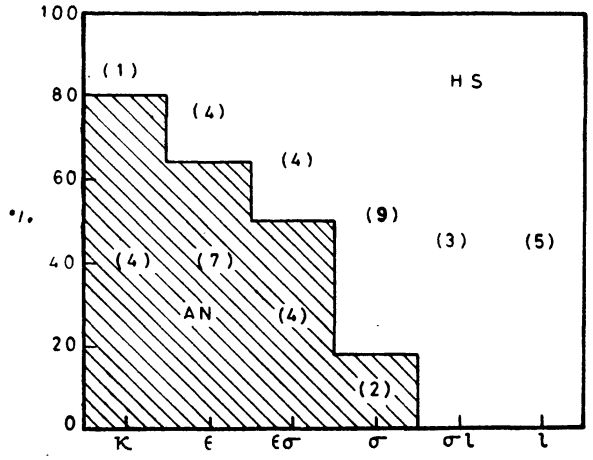

Figure 2. Distribution of Sérsic's classes AN and HS against the classification scheme presented in this paper.

The mean Yerkes type is *g* for class ϵ, *fg* for class σ and *af* for class ι (Prabhu 1979). Thus the central concentration decreases along our classification scheme.

A comparison of outer morphology with the inner structure reveals that the occurrence of barred or intermediate nature (*B*, *AB*) is higher in ϵ, $\epsilon\sigma$ and σ (90 per cent) as compared to $\sigma\iota$ and ι (63 per cent). The latter figure is comparable to the fraction of *A* and *AB* types (59 per cent) in the entire sample of spiral galaxies with $V_r \lesssim 5000$ km s^{-1} from de Vaucouleurs, de Vaucouleurs and Corwin (1976). The frequency of outer rings stays constant between the different classes (average: 20 per cent) but is higher than the corresponding figure for the entire sample (8 per cent). The distribution of the ' varieties ' *r*, *rs*, and *s* is not different from the larger sample, and does not show any variation between different classes. There is a systematic trend however in the mean Hubble type or the DDO luminosity class of each of our class (Prabhu 1979). As one moves from ϵ to ι the mean Hubble type changes from *Sab* to *Sc*; the luminosity class varies from I-II to III (We leave out class κ because of

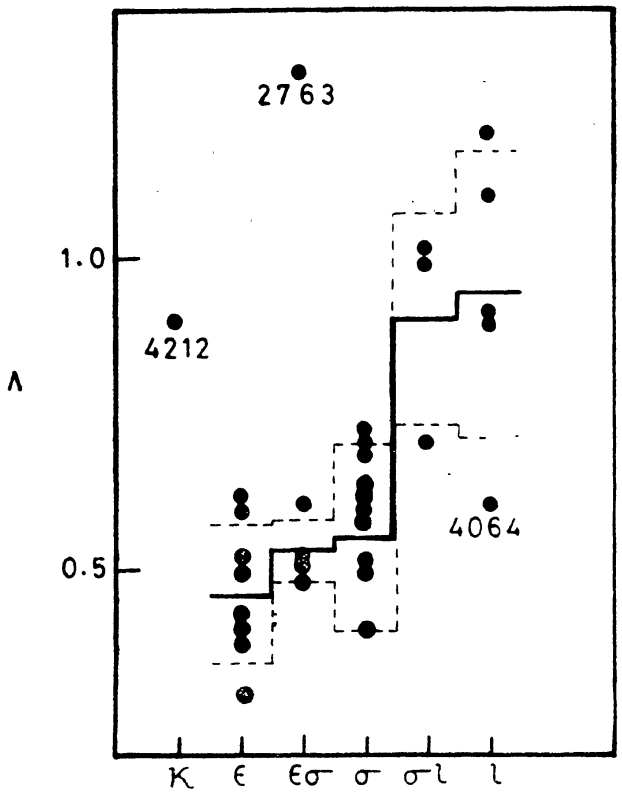

Figure 3. The distribution of the luminosity index of the parent galaxies as a function of the class of the central substructure. The solid line represents the mean luminosity index for each class and the dashed line one standard deviation limits on either side. NGC 2763 is excluded while obtaining the mean for class $\epsilon\sigma$. Galaxies which lie too far away from the mean are labelled.

the lack of statistics on luminosity class). This is as expected since the Hubble type and the DDO luminosity class are correlated. We show in Fig. 3 the distribution of de Vaucouleurs (1977) luminosity index $\Lambda = \frac{1}{10}(T+L)$ where T and L are Hubble type and DDO luminosity class respectively. It is evident from the figure that the classes σ and ι appear more often in low luminosity galaxies (higher Λ) while the classes ϵ, $\epsilon\sigma$ and σ prefer high luminosity ones.

It is significant that the formations of class ϵ generally present only absoprtion lines in their spectra (except for the emission of [O II] 3727Å). Among the central regions of 21 S-P galaxies observed spectroscopically by Prabhu (1978, 1979) all the class ϵ formations (NGC 210, 2196, 2935, 3627, 5850) failed to show H_α in emission. Among the remainder all but one (NGC 2763, Class $\epsilon\sigma$) showed the emission line of H_α. Other observations of class ϵ galaxies also do not show Balmer emission (NGC 4124: Sandage 1978; NGC 1433: de Vaucouleurs and de Vaucouleurs 1961). The only known exception is the class ϵ galaxy NGC 6951 (Burbidge 1962) which shows H_α though not the lines of [O III]. Published information exists on the presence of emission lines in many more non-ϵ class formations. The lack of emission lines in class ϵ makes their central regions appear redder than other systems both in $U-B$ and $B-V$ colours (Prabhu 1979). Corroborating the fact that no dust lanes are prominent in class ϵ formations we conclude that the gas and dust content and the number of hot stars are low in class ϵ systems.

4. Isophotometry

We present in this section the surface intensity distribution in integrated light (4000 Å–8700 Å) of the central regions of 27 S-P galaxies. These include six formations of type ϵ (NGC 210, 1300, 1433, 2196, 2935 and 3627), three of type $\epsilon\sigma$ (NGC 1326, 1415, 1672), ten of type σ (NGC 613, 1097, 1365, 1808, 2903, 2997, 3177, 3310, 3351, 5236), four of type $\sigma\iota$ (NGC 255, 922, 1087, 1140), three of type ι (NGC 3955, 4064, 7741) and one of type κ (NGC 1530).

Agfacontour Professional film was employed for obtaining the equidensity contours. The method has been explained by Geyer (1978). We have employed a yellow filter to narrow down the density width of a contour to 0·15 D in the first order and to 0·02 D in the second order. Third order contours were used only in isolated instances and were otherwise avoided because they add to the photometric noise. Fig. 4 shows the characteristic curve of the film as determined by us. The superposition of different pairs of contours was achieved by centering the contours of field stars.

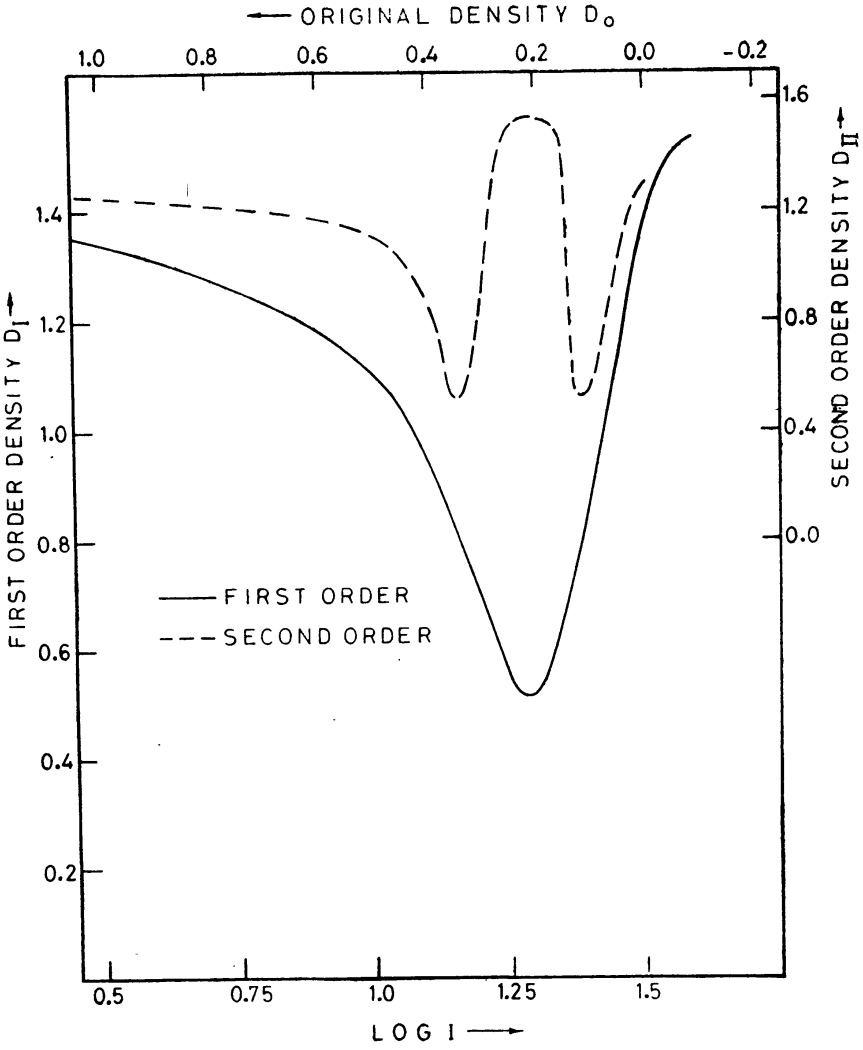

Figure 4. The first and the second order characteristic curves for the Agfacontour film obtained under conditions similar to the ones used in obtaining the equidensity contours.

The reductions to the relative intensity were achieved by reducing a microphotometer scan across the image of the galaxy, using a charactersitic curve obtained from the calibration plate. The orientation of the scan path was determined with the help of the field stars to an accuracy of 0°·1. It passed through the nucleus with an estimated accuracy of 10 μm (0·16 arcsec). The scanning aperture was

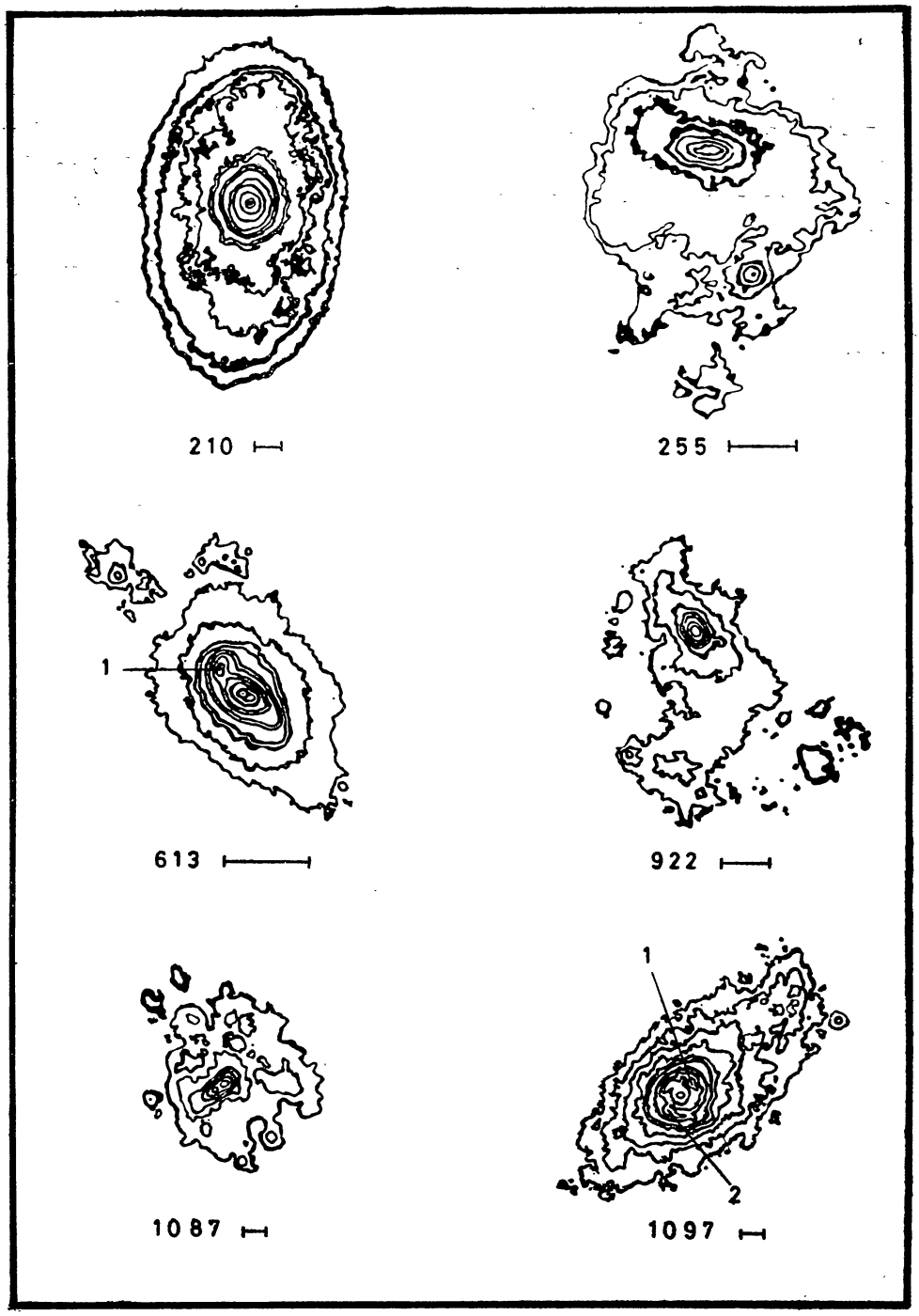

Figure 5a. The equidensity contours of S-P galaxies NGC 210, 255, 613, 922, 1087 and 1097. The lengths of the bars correspond to 10 seconds of arc in the sky. North is at the top and west is to the right. The relative brightness levels of different contours numbered centre outwards are listed in Table 2. The outermost two contours of NGC 210 are obtained from a published print and are not calibrated for intensity. The numbers in NGC 613 and 1097 designate regions discussed in Section 5.

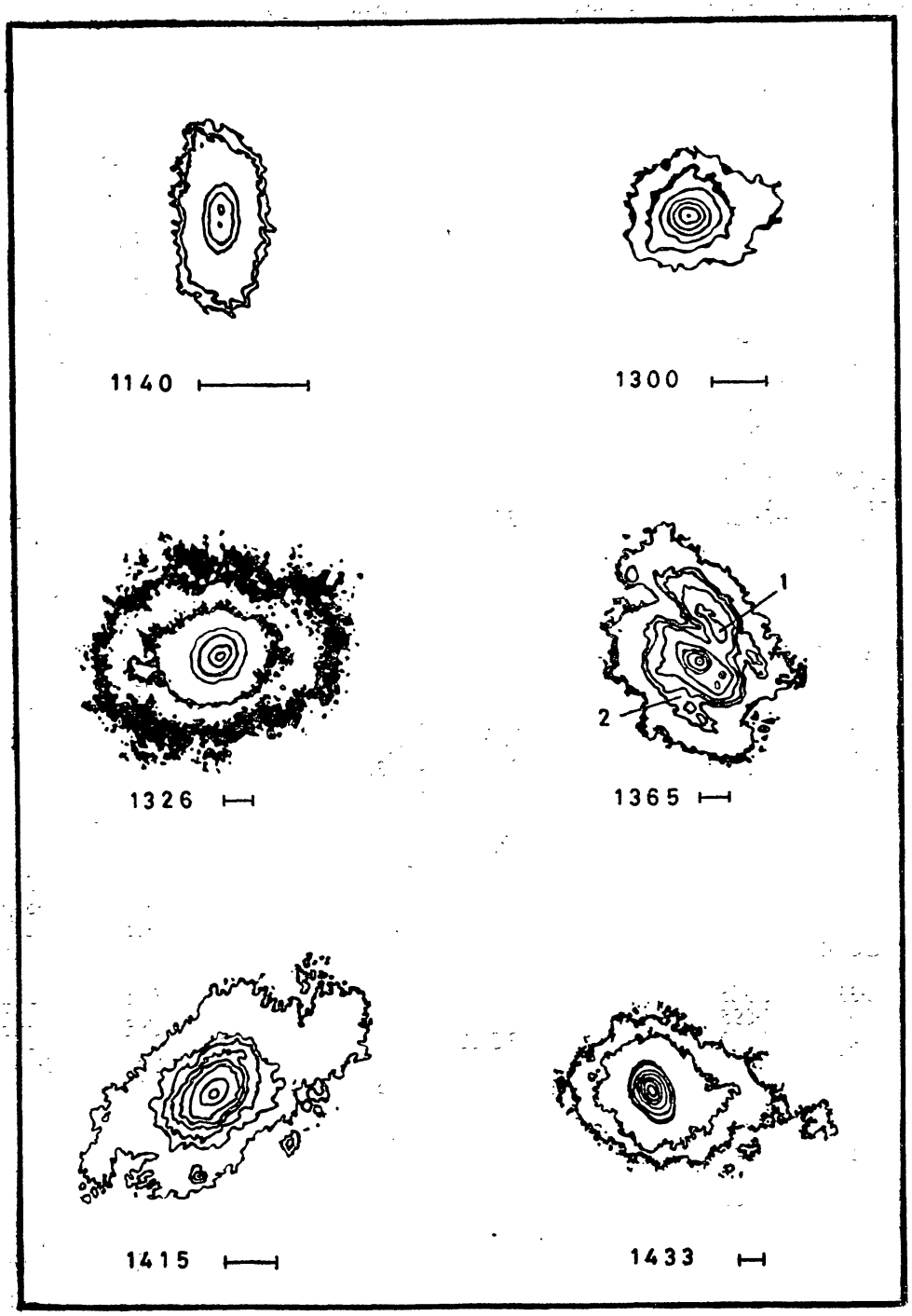

Figure 5b. The equidensity contours of the S-P galaxies NGC 1140, 1300, 1326, 1365, 1415 and 1433. Details are similar to Fig. 5a. The numbers in NGC 1365 designate the regions discussed in Section 5.

33 μm$\times$33 μm (0·5$\times$0·5 arcsec^2). Two different exposures were used in general. The internal accuracy was determined to be 0·05 mag which is partly due to the uncertainties of centering the scan path on the nucleus.

The equal intensity contours so obtained have been reproduced in Fig. 5. The intensities relative to the peak intensity have been listed in Table 2 for all the galaxies. The isophotes are designated outwards from the innermost contour. Some of the

Table 2. Equivalent luminosity profiles of the central regions of S-P galaxies.

No.	r^* arcsec	log I
	NGC 210	
1	0·61	0·747
2	1·25	0·569
3	2·74	0·140
*	3·03	0·121
4	4·33	−0·208
*	4·87	−0·247
5	6·21	−0·367
*	6·65	−0·526
6	7·41	−0·593
7	8·62	−0·628
8	10·79	−0·682
9+	11·75	−0·685
10	20·36	−0·738
11	25·65	−0·757
	NGC 255	
1	1·17	0·976
2	2·01	0·880
3	2·95	0·692
4	4·22	0·538
5+	6·96	0·308
6	14·77	0·052
7	19·41	−0·009
	NGC 613	
1	0·33	0·985
2	0·73	0·895
3	1·41	0·833
4	2·13	0·807
5	2·71	0·698
6	3·89	0·559
7	5·16	0·547
8+	5·79	0·480
9	7·96	0·350
10	11·71	0·100
	NGC 922	
1	1·95	0·815
2	2·46	0·630
3	3·58	0·450
4	4·28	0·280
5+	5·96	0·210
6	11·90	0·135
7	24·11	0·075
	NGC 1087	
1	1·11	0·943
2	1·62	0·828
3+	1·95	0·785
4	2·77	0·642
5	3·88	0·550
6	5·61	0·422
*	8·63	0·405
	NGC 1097	
1	1·71	0·715
2	5·65	0·425
*	6·82	0·298
3	10·27	0·137
*	10·98	0·090
4	12·53	0·059
*	13·55	−0·003
5	17·07	−0·115
6+	18·87	−0·135
7	23·55	−0·205
8	29·54	−0·280
9	39·92	−0·300
10	51·94	−0·396
	NGC 1140	
1	0·34	0·959
2	1·97	0·725
3	2.69	0·544
4	6·43	0·135
5+	7·36	0·107
	NGC 1300	
1	0·00	1·000
2	2·83	0·701
3	4·36	0·597
4	5·61	0·482
5	8·44	0·373
6+	12·01	0·193
7	19·17	0·111
	NGC 1326	
1	1·23	0·893
2	3·10	0·724
*	4·50	0·555
3	5·68	0·380
4+	8·05	0·190
5	15·83	0·002
6	29·17	−0·148
	NGC 1365	
1	0·00	1·000
2	1.00	0·851
3	2·11	0·641
4	2·75	0·544
5	5·69	0·376
6+	8·46	0·214
*	9·12	0·193
7	11·38	0·124
8	13·24	0·083
9	19·97	0·017
	NGC 1415	
1	1·81	0·670
2	2·62	0·583
*	2·82	0·560
3	3·15	0·368
*	3·50	0·345
4	6·45	0·242
5	7·38	0·192
6+	9·22	0·152
7	11·46	0·142
8	21·76	0·042
	NGC 1433	
1	2·31	0·820
*	2·61	0·798
2	4·50	0·635
*	4·68	0·620
3	5·46	0·575
*	6·03	0·561
4	8·12	0·499
*	8·37	0·438
5	10·74	0·310
6+	13·07	0·213
7	30·48	0·119
8	43·80	0·069

The contours marked with an asterisk (*) are not shown in Figure 5. The + signs designate the contours at which the luminosity profile changes slope.

Table 2. continued

No.	r^* arcsec	log I
	NGC 1530	
1	1·49	0·889
*	2·13	0·810
*	3·04	0·693
2+	4·03	0·643
3	7·36	0·583
*	8·26	0·563
*	10·15	0·513
4+	13·37	0·491
5	34·76	0·403
	NGC 1672	
1	0·40	0·965
2	3·01	0·947
*	3·62	0·776
*	4·84	0·628
3	5·73	0·556
*	8·33	0·487
4+	8·84	0·297
5	19·38	0·132
6	36·78	0·122
	NGC 1808	
1	0·51	0·958
2	1·70	0·783
3+	4·73	0·630
4	6·60	0·263
5+	10·96	0·153
	NGC 2196	
1	0·47	0·922
2	2·11	0·597
3	5·54	0·504
4	9·07	0·367
5+	18·80	0·056
6	34·58	0·006
	NGC 2903	
1	0·40	0·950
2	1·45	0·833
3	2·92	0·728
4	5·05	0·652
5	6·23	0·600
6	8·89	0·450
7	12·25	0·385
8+	13·58	0·380
	NGC 2935	
1	0·32	0·980
2	0·78	0·870
3	2·42	0·702
4	3·07	0·602
5	3·35	0·503
6	4·51	0·419
7	5·24	0·297
8	5·83	0·262
9+	11·05	0·092
10	16·25	0·065
	NGC 2997	
1	0·69	0·897
2	1·47	0·759
3	2·68	0·614
4	4·37	0·567
5	5·29	0·457
*	6·22	0·422
6	8·77	0·292
7+	15·67	0·177
	NGC 3177	
1	0·45	0·838
2	1·55	0·588
3	2·54	0·513
4+	8·09	0·383
	NGC 3310	
1	1·62	0·676
*	1·77	0·522
2	2·57	0·322
3+	4·60	0·215
4	8·69	0·188
5	9·48	0·082
6	10·01	0·066
7	11·19	0·007
8	12·67	−0·013
9+	17·77	−0·039
	NGC 3351	
1	0·46	0·956
2	1·29	0·906
*	1·80	0·832
3	2·51	0·778
*	3·76	0·565
4	4·15	0·488
5	5·01	0·408
6	6·02	0·328
7	7·65	0·278
8+	10·95	0·178
	NGC 3627	
1	1·61	0·825
2	1·94	0·762
*	3·43	0·584
3	3·64	0·569
4	6·54	0·377
5+	7·71	0·353
6	11·14	0·227
7	13·06	0·175
8+	20·14	0·142
9	22·56	0·102
*	43·51	−0·043
*	58·36	−0·063
	NGC 3955	
1	1·51	0·973
2	2·24	0·925
3	4·98	0·858
4	5·78	0·790
5	10·92	0·680
6+	12·66	0·665
	NGC 4064	
1	0·86	0·985
2	2·62	0·910
*	3·33	0·889
3	3·50	0·855
4	4·13	0·805
5+	8·19	0·732
6	10·99	0·690
	NGC 5236	
1	3·38	0·625
2	5·40	0·370
3	7·36	0·090
4+	11·31	−0·135
	NGC 7741	
1	0·42	0·965
2	1·76	0·948
3	3·40	0·900
4	5·11	0·872
*	6·61	0·860
5+	7·04	0·835

The contours marked with an asterisk (*) are not shown in Figure 5. The + signs designate the contours at which the luminosity profile changes slope.

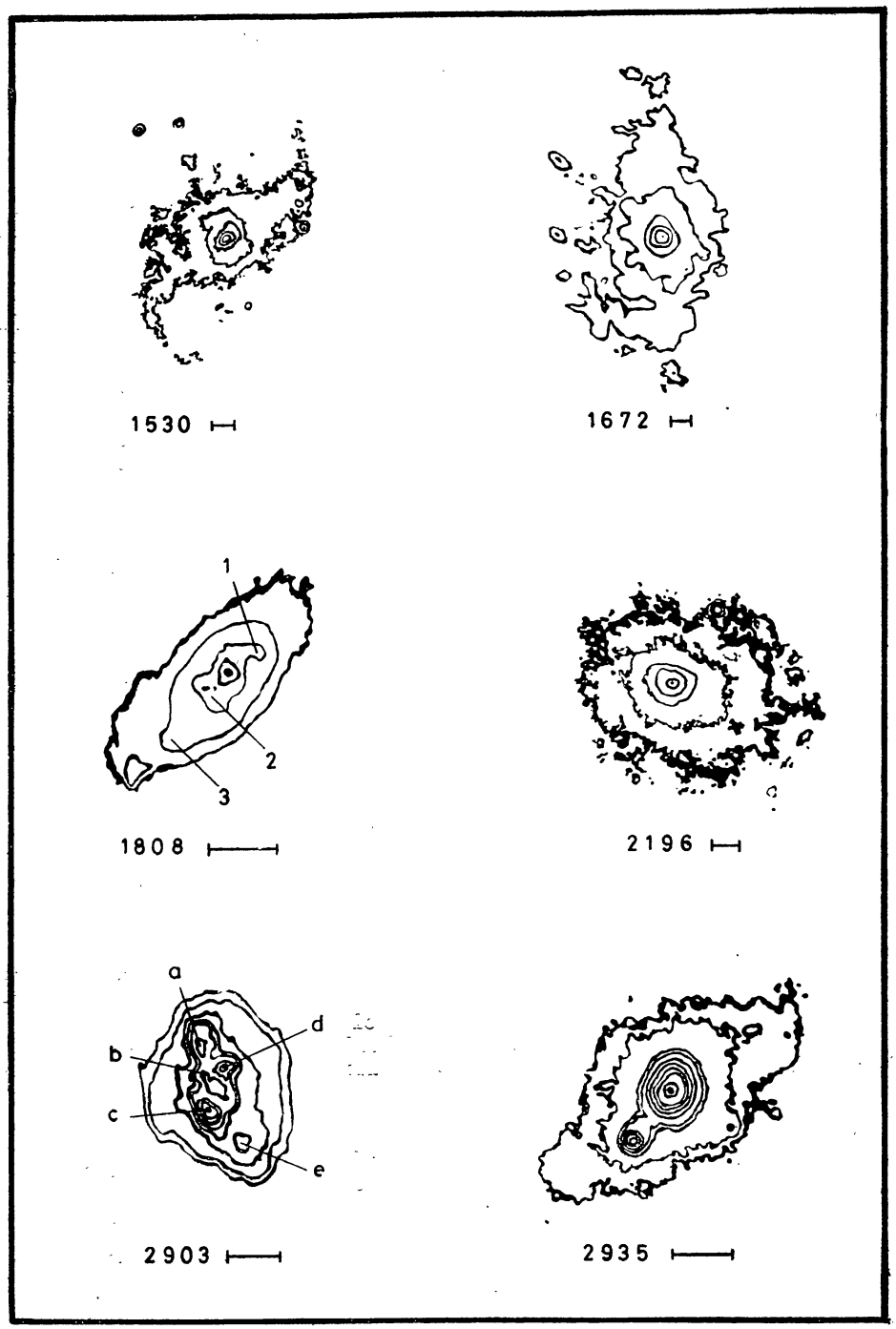

Figure 5c. The equidensity contours of the S-P galaxies NGC 1530, 1672, 1808, 2196, 2903 and 2935. Details are similar to Fig. 5a. The numbers in NGC 1808 and the letters in NGC 2903 designate regions discussed in Section 5.

contours obtained have not been reproduced in the figure to avoid overcrowding; their parameters appear in the table without any numerical designation. Listed also in Table 2 are the equivalent radii $r^*=(A/\pi)^{1/2}$ where A is the area of a particular isophote in square seconds of arc. The equivalent radius can be treated as an average radius when a single contour represents a given intensity level. Some galaxies of

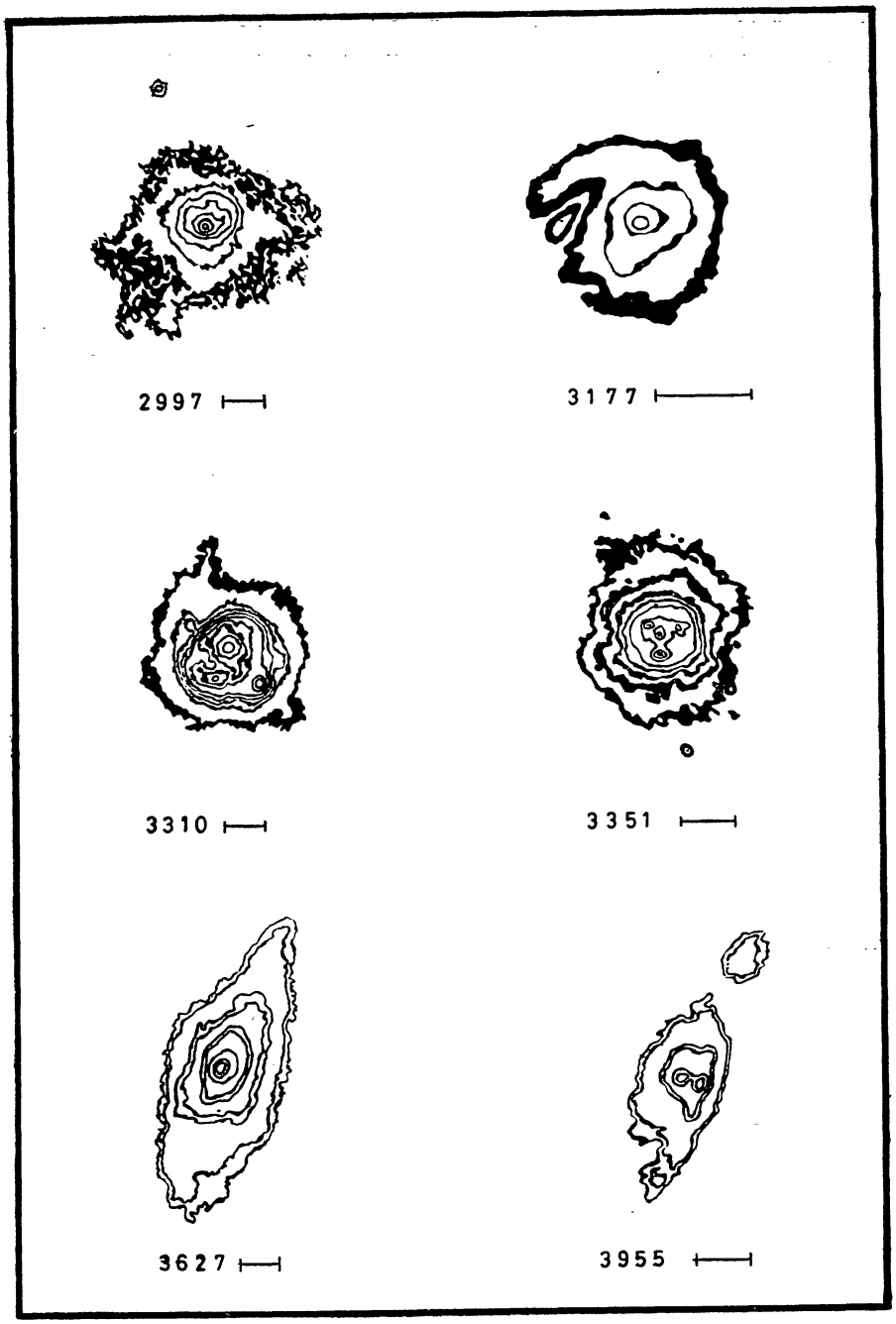

Figure 5d. The equidensity contours of the S-P galaxies NGC 2997, 3177, 3310, 3351, 3627 and 3955. Details are similar to Fig. 5a.

class σ exhibit distinct hot-spots even in the integrated light and hence possess different unconnected contours at a given intensity level; in such a case the equivalent radius is related only to the total area, with the surface brightness above a given value. Smooth curves through the points listed in Table 2 appear in Fig. 6. The photometric noise was smoothened whenever present. This noise arises whenever third order isophotes were used and a few times even in the second order isophotes.

Its effect is seen in some of the isophotes in Fig. 5 that appear similar to each other in pairs (*e.g.* NGC 1140). It is desirable to use the mean isophote in such situations.

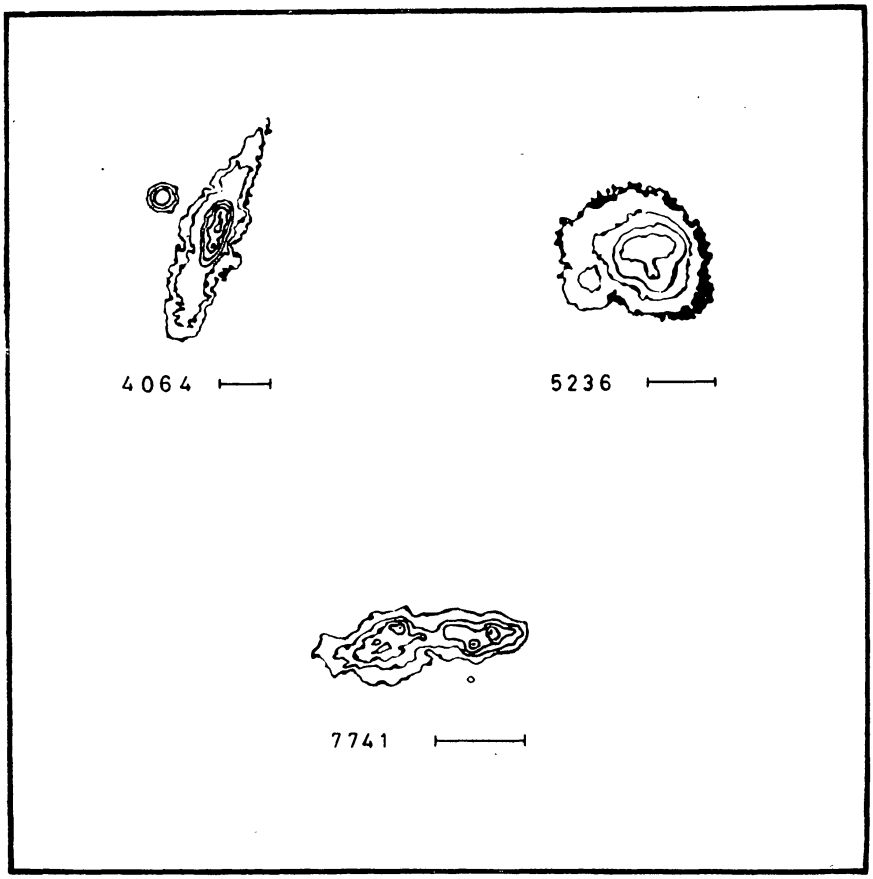

Figure 5e. The equidensity contours of the S-P galaxies NGC 4064, 5236 and 7741. Details are similar to Fig. 5a.

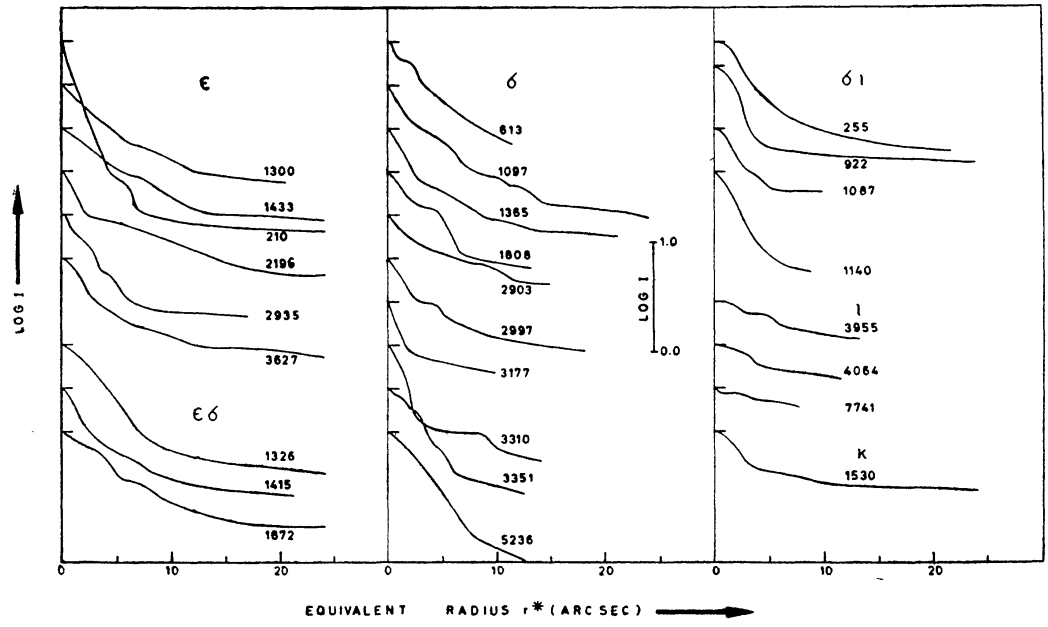

Figure 6. The relative equivalent luminosity profiles for the 27 S-P galaxies. The relative intensity scale is shown in the central frame.

The luminosity profiles in Fig. 6 are only on a relative scale of intensity. As already mentioned in Section 2, we have used the entire band (4000 Å–8700 Å) of the image tube response in our observations so as to integrate the contribution from the hot spots as well as the stellar population, and to reduce the contrast of the dust lanes. It is hence not possible to establish an accurate zero point for the luminosity profiles. We have, however, compared our profiles with the inner overlapping regions of the blue luminosity profiles of Sérsic (1968) whenever available (Table 4 in Section 6). We have also compared the profiles of Sérsic with the photoelectric *B* magnitudes of Alcaino (1976) with a 5·5 arcsec aperture. The agreement is generally good between the profiles (except that the blue profiles are slightly steeper than ours) and also between the profiles of Sérsic and the photometry of Alcaino. The mean surface brightness seen through a 5·5 arcsec aperture is $1{\cdot}4 \pm 0{\cdot}6$ mag fainter than the peak surface brightness obtained by overlapping our profiles with those of Sérsic. The agreement is not good in the case of NGC 1672: the peak surface brightness is 1·6 mag fainter than the average surface brightness through the 5·5 arcsec aperture. The discrepancy probably results partly from the poor seeing on our photographs of this highly southern object and partly from overexposure of inner regions in Sérsic's photometry. A peak brightness of 18·0 mag arcsec^{-2} is a more likely value.

5. Colour distribution

Six galaxies were photographed in two spectral bands as explained in Section 2. We denote these bands by *BL* (4000 Å–4600 Å) and *IR* (7000 Å–8700 Å). We chose one galaxy of class ϵ (NGC 210) and five of class σ (NGC 613, 1097, 1365, 1808 and 2903). The photographs were scanned to derive radial profiles in a single direction. The profiles have been obtained in two different directions for NGC 2903 because in this case the hot spots are extremely distinct. The profiles in *BL*, *IR* and in the (*BL-IR*) colour are presented in Fig. 7. The intensities as well as the colours are in relative units. The scans cover the perinuclear regions and the extreme points are barely outside the perinuclear component.

The colours at the extremities of the profiles do not agree with each other in the cases of NGC 1097, 1365 and the P.A. 168° profile of NGC 2903. The south-eastern regions of NGC 1097 and 1365 are redder than the north-eastern regions while in NGC 2903 it is the north-eastern region that is redder. The most prominent feature in all the profiles is, however, a red nucleus. Relative to the region surrounding the bright perinuclear formations (a bar or a lens) the nuclei are redder by Δ (*BL-IR*)=0·8 mag in NGC 210 and 1365, by $\sim$ 0·4 mag in NGC 613, 1097 and 1808, while the nucleus of NGC 2903 is 0·6 mag redder. The observations of NGC 2903 correspond to the nucleus identified by Prabhu (1980). The nuclei of NGC 1097 and 1808 are not very prominent in the colour profiles partly since the entire perinuclear formation is red. The perinuclear region of NGC 1365 also exhibits some degree of reddening. The ridge 2 (*cf.* Figs 5 and 7) south-east of the nucleus and visible in the blue is not visible in the red. The hot spots are generally bluer by —0·2 to —0·4 mag in all the galaxies (*cf.* 1 in NGC 613, 1 in NGC 1365 and *c* in NGC 2903), a fact that suggests that the hot spots that appear neutral or redder are reddened by dust (*e.g.* all the hot spots in NGC 1097, 1808 and *a*, *b* in NGC 2903).

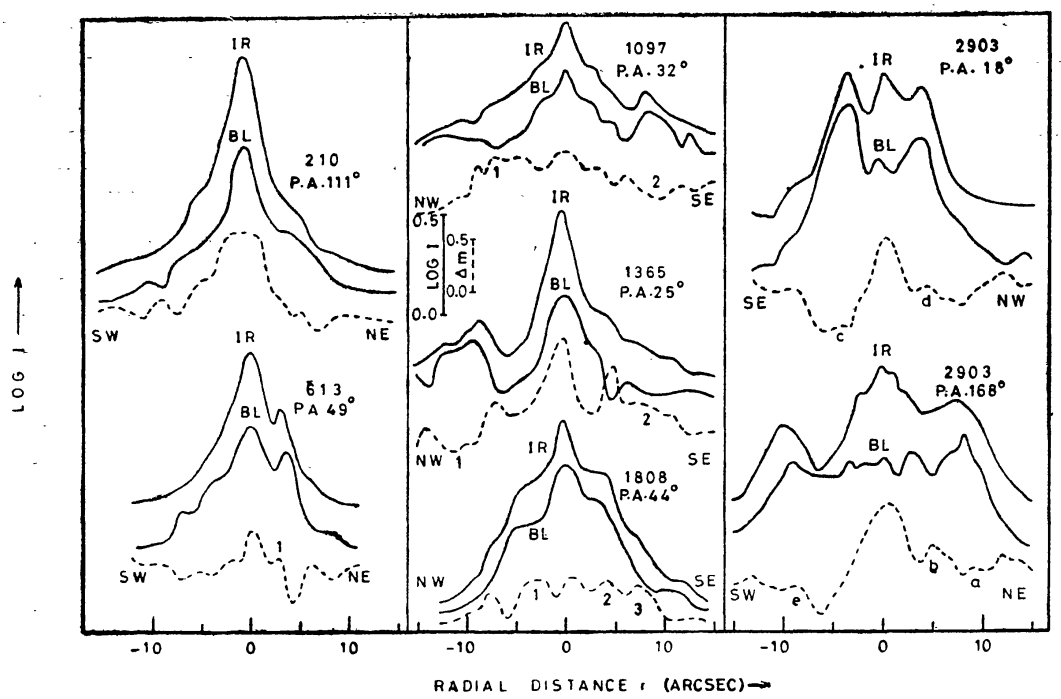

Figure 7. The intensity scans across the central regions of different S-P galaxies. The continuous lines are in *IR* (7000Å–8700Å) and *BL* (4000Å–4600Å) bands while the dotted lines show the *BL-IR* intensity difference on a magnitude scale. The scales are shown in the central frame. The zero point is arbitrary. Note the faintness of the nucleus of NGC 2903 in *BL*. Numbers and letters designate individual regions discussed in the text.

6. Geometrical and photometric properties

The geometrical and photometric properties derived from the photographs and the luminosity profiles appear in Table 3. The galaxies are grouped according to the classification of the central regions. The galaxy type in column 2, the luminosity index in column 3 and the axial ratio in column 4 are all taken from de Vaucouleurs, de Vaucouleurs and Corwin (1976). The heliocentric radial velocities in column 5 are also taken either from the same source or from Sandage (1978) when not available in the former. The radial velocity of NGC 4250 is from Kelton (1980) and that of NGC 3956 is based on a low dispersion plate obtained by the author at the Kavalur Observatory. The semimajor axis a in seconds of arc (column 6) and the axial ratio ρ (column 7) are derived from direct measurements on the plates. The measurements were performed at the points where the surface brightness drops off sharply. All Sérsic-Pastoriza galaxies have by definition, such a sharp drop in luminosity at the edge of the perinuclear component that it is fairly easy to measure the sizes without any exposure-dependent systematic errors. The contours nearest to such a drop are marked in Table 2. The sizes of the star-like nuclei are also measured in several cases and appear in Table 3 with a subscript n after the NGC designation. The perinuclear component in class κ is too faint and hence could not be measured in all the cases. The length of the semimajor axis was converted to a linear scale assuming a uniform Hubble flow with a constant $H_0=50$ km s^{-1} Mpc^{-1} and appear as a_{kpc} in column 8. We propose that the apparent nucleus of NGC 7769 consists of

Table 3. Classification of central regions of S-P galaxies and their geometrical and photometric properties.

NGC	Type	A	Log R	V_0	log a	log ρ	a_{kpc}	log L (kpc)	m_b-m_p	$m_b-m_p^0$
1	2	3	4	5	6	7	8	9	10	11
Class κ:										
1530	SBT3		0·23		1·325	0·22			1·35	0·98
1530 n					0·743	0·06				
3504 n	RSXS2		0·09	1479	0·701	0·15	0·72			
3611	SAS1P		0·07	1603	1·028	0·12	1·66			
3611 n					0·559	0·00	0·56			
4151 n	PSXT2*		0·13	1002	0·747	0·01	0·54			
4212 n	SA4S	0·9	0·16	1947	0·656	0·00	0·86			
4250 n	LXR+		0·11	2106b	0·521	0·02	0·68			
7769	RSAT3		0·01	4570	0·559	0·02	1·61			
Class ε:										
210	SXS3	0·4	0·16	1700	1·149	0·15	2·32	1·25	4·30	4·28
1300	SBT4	0·5	0·18	1422	0·911	0·12	1·12	1·33	2·25	2·10
1433	SBR1		0·05	802	1·212	0·35	1·27	1·10	2·17	2·01
2196	PSAS1	0·3	0·10	2080	0·822	0·11	1·34	1·64	2·50	2·39
2935	PSXS3	0·4	0·08	1939	0·980	0·18	1·80	1·21	2·27	2·13
3627	SXS3	0·6	0·30	583	1·511	0·37	1·83	1·24	2·57	2·46
3627 n					1·036	0·16	0·61			
4124	LAR+		0·42	1551a	1·293	0·29	2·95			
4245	SBRO*	0·5	0·10	882	1·033	0·10	0·92			
4245 n					0·540	0·04	0·30			
5850	SBR3	0·4	0·04	2354	1·071	0·11	2·69			
6951	SXT4	0·6	0·06	1627	0·877	0·22	1·19			
7410	SBS1		0·43	1634	0·591	0·05	0·62			
Class εσ:										
1326	RLBR+		0·12	1167	1·085	0·13	1·38	1·42	2·90	2·82
1415	RSXSO	0·5	0·24	1399	1·048	0·29	1·52	1·30	2·37	2.24
1672	SBS3	0.5	0·09	1076	0·971	0·01	0·98	1·16	2·17	2·01
2763	SBR6P	1·3	0·04	1634	0·957	0·21	1·44			
4258	SXS4		0·36	537	1·235	0·36	0·89			
5248	SXT4	0·5	0·12	1102	1·243	0·26	1·87			
5597	SXS6		0·06	2573a	0·822	0·12	1·66			
6907	SBS4	0·6	0·06	3238a	0·735	0·11	1·71			
7552	PSBS2		0·15	1636	0·934	0·15	1·36			
Class σ:										
613	SBT4	0·6	0·10	1462	0·952	0·25	1.27	1.28	2·40	2.27
1097	SBS3	0.5	0.15	1227	1.048	0.01	1.33	1.51	3.25	3.19
1365	SBS3	0.5	0.25	1502	1.240	0.28	2.53	1.35	2.50	2.39
1808	RSXS1		0.25	769	1.299	0.33	1.48	0.85	2.20	2.05
1808 n					0.656	0.19	0·34			
2903	SXT4	0.6	0.28	467	1.293	0·46	0·89	0·73	1·63	1·35
2997	SXT5	0·6	0·10	805	1·240	0.31	1·36	0·97	2·07	1·90
3177	SAT3	0·7	0·09	1123	1·170	0·15	1·61	0·54	1·45	1·12
3177 n					0·877	0·03	0·82			
3310	SXR4P	0·7	0·09	1063	1·325	0·17	2·18	1·14	2·65	2·55

Table 3. *Continued*

NGC	Type	Λ	Log R	V_0	log a	log ρ	a_{kpc}	log L (kpc)	m_b-m_p	$m_b-m_p^0$
1	2	3	4	5	6	7	8	9	10	11
3310 n					0·656	0·00	0·47			
3351	SBR3	0·6	0·16	673	1·120	0·04	0·86	0·86	2·17	2·01
5236	SXS5	0·7	0·04	337	1·187	0·11	0·50	0·93	3·77	3·74
5728	SXR1*	0·4	0·24	2879a	0·877	0·08	2·10			
Class σ_t:										
255	SXT4	0·7	0·05	1873	1·044	0·56	3·01	1·56	2·65	2·55
922	SBS6P	1·0	0·04	3010a	0·895	0·30	2·29	1·27	1·67	1·41
1087	SXT5	1·0	0·17	1844	0·980	0·39	1·71	0·99	1·47	1·15
1140	I 9		0·23	1503	0·985	0·31	1·41	1·12	2·45	2·33
4369	RSAT1		0·01	1066	1·092	0·33	1·28			
Class t:										
925	SXS7	1·1	0·21	716	1·272	0·68	1·30			
3206	SBS6		0·15	1245	1·011	0·25	1·24			
3346	SBT6	0·9	0·05	980a	0·942	0·45	0·83			
3955	I 0		0·39	1118	1·204	0·17	1·73	0·96	0·83	0·14
3956	SAS5*	1·2	0·45	726c	1·286	0·33	1·36			
4064	SBS1*P	0·6	0·36	959	1·116	0·26	1·21	0·68	0·67	−0·16
7741	SBS6	0·9	0·15	1018	1·088	0·75	2·41	0·36	0·25	−1·47

References to radial velocities:
(a) Sandage (1978)
(b) Kelton (1980)
(c) Prabhu (unpublished)

the entire perinuclear region that appears star-like owing to its great distance. On the other hand the nucleus of the nearby galaxy, NGC 5236, is so well resolved that it appears like the perinuclear component.

Derivation of photometric properties for a two component system is extremely complex and is further complicated when a bar or a lens is present (Kormendy 1980). Hence, we will not attempt a decomposition of the observed profile into different components, but directly intercompare the observed profiles of different galaxies. We assume in the following that the bars and lenses are equivalent (Kormendy 1979) and that the outermost parts of all the luminosity profiles presented in Section 4 are dominated by this component. We assume further that the luminosity profiles of all the bars have similar shape and can be matched with each other after proper scaling in length and intensity. We have converted the observed profiles to a linear scale in size (H_0=50 km s^{-1} Mpc^{-1}) and scaled them to match the bar dominated region. We compared these scaling factors with the bar lengths published by Kormendy (1979) or measured by us on published photographs for eight galaxies (NGC 613, 1097, 1300, 1365, 1433, 2997, 3351 and 5236). The relationship was linear and provided the necessary zero point. The estimates of the bar lengths L derived from this relation are listed for 26 galaxies in column 9 of Table 3. We prefer this scale length to the actual bar length L_0 since L is a photometrically derived parameter and is less affected by subjective errors of measurement.

We proceed to obtain the peak central surface brightness relative to the surface brightness of the bar just outside the perinuclear component. These values, m_b-m_p

appear on a magnitude scale in column 10 of Table 3. If the contribution of the central surface brightness of the bar to m_p is removed using the relationship

$$m_p^0 = -2{\cdot}5 \log [\text{dex}\,(-0{\cdot}4\, m_p) - \text{dex}\,(-0{\cdot}4\, m_b)],$$

we obtain the peak surface brightness of the central formation m_p^0. The value of $m_b - m_p^0$ appear in column 11 of Table 3.

We can draw a few important statistical conclusions from the photometric and structural parameters in Table 3.

6.1 *Sizes of the Nuclei and the Perinuclear Components*

The histogram in Fig. 8 shows the distribution of the structures of different semi-major axes. Mean size of the star-like nuclei is $0{\cdot}68 \pm 0{\cdot}35$ kpc while that of the perinuclear components (hatched area) is $1{\cdot}56 \pm 0{\cdot}65$ kpc. If the perinuclear component is barlike (*cf.* Section 6.2) oriented randomly in the plane of the galaxy the

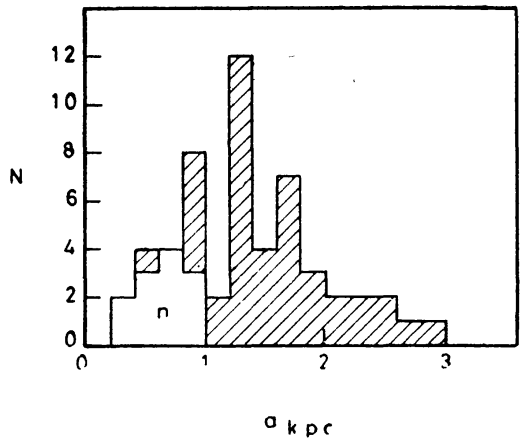

Figure 8. Histogram showing the distribution of the semi major axes of the central substructures in different S-P galaxies.

above average is an underestimate while the dispersion is an overestimate. There is no significant correlation between the size of the perinuclear component and the bar length. The correlation coefficient is 0·19 if the major axis is used, and improves to 0·33 if the geometric mean of the semimajor and semiminor axes is used.

6.2 *Shapes of the Nuclei and the Perinuclear Components*

The isophotes in Fig. 5 show that the position angles of the major axes and the ellipticities of the perinuclear formations differ quite often from the similar quantities for the outer regions. Most striking examples are NGC 1433 and NGC 2935. Such configurations arise in either of the following situations: (a) if the perinuclear formation is barlike (b) if the perinuclear formation is a disk with its plane tilted with respect to the plane of the parent galaxy. We favour the first of these hypotheses as the latter faces the angular momentum problem.

A more quantitative evidence for the barlike structure of the perinuclear formations comes from the distribution of the axial ratios of the formations with respect to the axial ratios of the parent galaxies. We assume that the parent galaxy is a disk with an axial ratio R resulting from its inclination to the line of sight. With ρ as the observed axial ratio of the perinuclear component we expect the following relations to hold for different geometrical structures:

thin disk:	$\log \rho = \log R$
thick disk or oblate spheroid:	$\log \rho < \log R$
sphere:	$\log \rho = 0.$

If the geometrical structure is a prolate spheroid with the major axis oriented randomly in the plane of the disk of the galaxy, the relationship between $\log \rho$ and $\log R$ would be very weak.

We plot in Fig. 9 the inner and the outer axial ratios for all the observed galaxies.

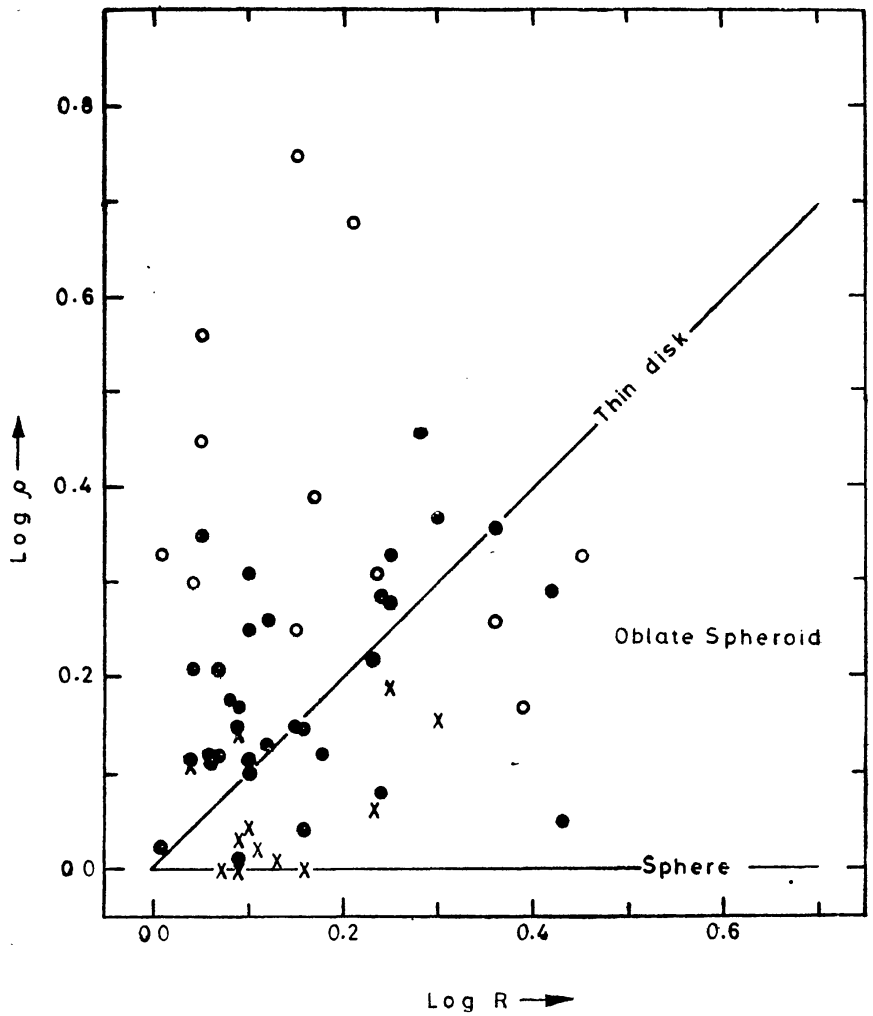

Figure 9. The distribution of the axial ratios of the central substructures (ρ) and the axial ratios of the parent galaxies (R) on a logarithmic scale. The filled circles are the perinuclear formations of classes κ, ϵ, $\epsilon\sigma$ and σ. The open circles represent classes σ_ι and ι. Crosses denote the nuclei. The expected positions for thin disks and spheres are shown by straight lines. The oblate spheroids should be contained by these lines.

The perinuclear formations of classes $\sigma\iota$ and ι are represented by open circles while for the remaining classes a filled circle is used. The crosses represent the star-like nuclei. The straight lines for thin disk and spheres are shown. The oblate spheroids are included by these lines. The prolate spheroids may lie anywhere in the diagram. The longer the major axis with respect to the minor axis, the higher above the ' thin disk ' line would be the mean position of prolate spheroids. It is obvious from the figure that the perinuclear formations of classes $\sigma\iota$ and ι are certainly barlike. It is highly likely that the formations of classes ϵ, $\epsilon\sigma$, σ and κ possess barlike distortions too judging from the large scatter among the points representing these objects. The mean departures from the ' thin disk ' line for these systems are:

$$\log \rho - \log R = 0{\cdot}03 \pm 0{\cdot}13 \text{ for } \kappa, \epsilon, \epsilon\sigma \text{ and } \sigma \ (n = 33)$$

$$= 0{\cdot}21 \pm 0{\cdot}27 \text{ for } \sigma\iota \text{ and } \iota \qquad (n = 12).$$

The description in Section 3 of the regularity in the structure of the perinuclear component supports the view that the scatter diagram in Fig. 9 does not result from the stochastic distribution of hot spots in the central regions, but indicates a real departure of the structure from cylindrical symmetry. All the axial ratios of the parent galaxies have mean errors in log R smaller than 0·045 and often better than 0·025. Hence the errors in log R do not contribute significantly to the scatter. Thus an overwhelming part of the scatter in the figure is real.

The nuclei are generally close to the ' sphere ' line in Fig. 9 and lie within the region of the oblate spheroids with the exceptions of NGC 3504 and 5236. They have a mean axial ratio of

$$\log \rho = 0{\cdot}06 \pm 0{\cdot}07 \qquad (n = 12).$$

They are probably spherical or oblate in shape. It should be borne in mind, though, that image smearing due to seeing makes them appear more circular than what they actually are.

6.3 *Brightness of the Perinuclear Formations*

Sorensen, Matsuda and Fujimoto (1976) have suggested that the bar potential in a barred galaxy dissipates the angular momentum of the gas in the disk and condenses it to the centre. They expect this mechanism to be more efficient as compared to the dissipation of the angular momentum by the spiral density wave. The observation that the overwhelming majority of Sérsic-Pastoriza galaxies are barred or intermediate supports this view. There are seven galaxies listed in Kormendy (1979) with bars exceeding a length of about 20 kpc: NGC 613, 1097, 1300, 4593, 5383, 5850 and 7479. Note that all but the last one is in the list of Sérsic (1973).

If the supply of gas to the inner regions of S-P galaxies is caused by the bar, we would expect a correlation between the length of the bar and the central activity. We list in Table 4 the lengths of the bars for seven galaxies for which we have the approximate photometric zero point as obtained in Section 4. We have also added NGC 4314 for which photometric parameters are taken from Benedict (1980). The bar

Table 4. Central surface brightness of the bars and the perinuclear formations.

NGC	Bar length L_0 (arcmin)	log L_0 (kpc)	m_p mag arcsec^{-2}	$m_b - m_p$ mag	m_b mag arcsec^{-2}	m_p^0
1	2	3	4	5	6	7
613	2·3 K	1·29	17·7	2·4	20·1	17·8
1097	3·0 K	1·39	16·9	3·3	20·2	17·0
1365	3·0 T	1·40	16·7	2·5	19·2	16·8
1433	2·8 T	1·12	18·1	2·2	20·3	18·2
1672	3·0 T	1·27	19·9	2·2	22·1	20·0
			18·0a		20·2a	18·1a
2997	2·0 T	0·98	18·7	2·1	20·8	18·8
4314	2·1 T	1·03	18·2b	2·0b	20·2	18·3
5236	5·0 T	0·98	15·1	3·8	18·9	15·1
			18·9	1·6c	20·5c	18·6

Notes: K Kormendy (1979)
T This work
a Corrected as mentioned in Section 4
b Benedict (1980)
c Talbot, Jensen and Dufour (1979)

lengths in column 2 are either taken from Kormendy (1979) or measured on published photographs. Columns 3 and 4 give the absolute length of the bar L_0 (kpc) and the peak surface brightness m_p of the central region of the galaxy. The difference between the central surface brightness of the bar and the peak surface brightness $m_b - m_p$, in column 5 is taken from Table 3. The central surface brightness of the bar m_b appears in column 6. The peak surface brightness of the perinuclear component m_p^0 is derived as explained earlier in this section.

We have listed two values each of m_p, m_b and m_p^0 for NGC 1672 and 5236. The effect of poor resolution on NGC 1672 is discussed in Section 4 and the second value for this galaxy is a value corrected for this effect. NGC 5236 is a counter example for the same effect. It is the closest galaxy in our sample and hence provides a very high spatial resolution. The entire region observed by us has the dimensions of the star-like nuclei in the remaining galaxies. Thus the peak brightness is that of the nuclear region alone. The perinuclear region dominates the profile after $r^* \sim 10$ arcsec, and has a central brightness of 18·9 mag arcsec^{-2}. We have not been able to observe the bar in this galaxy which has a surface brightness of 20·5 mag arcsec^{-2} as seen from the surface photometry of Talbot, Jensen and Dufour (1979). The values with these assumptions appear in the second row for NGC 5236.

We plot in Fig. 10a the values of corrected peak surface brightness m_p^0 against the logarithmic bar length. A correlation is evident in the sense that longer bars have brighter perinuclear components. The corrected values for NGC 1672 and 5236 are shown by filled squares. The straight line

$$m_p^0 = 23{\cdot}90 - 5 \log L_0 \text{ (kpc)},$$

fits the observed points well. The relation implies, that the peak surface brightness of the perinuclear component varies as the square of the bar length. Since the area

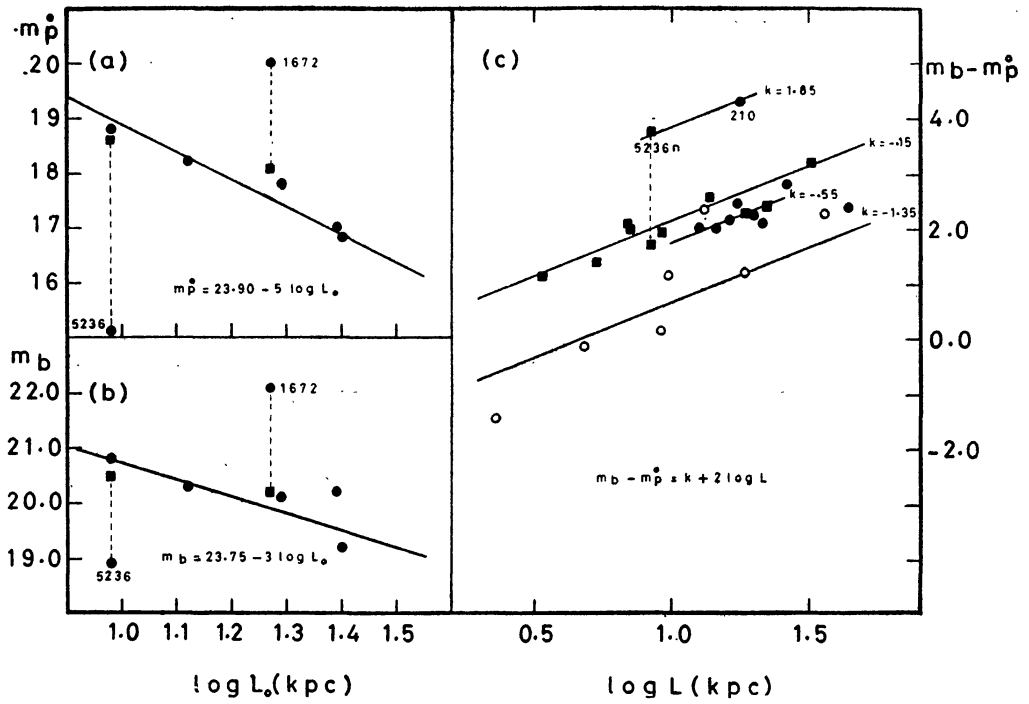

Figure 10. The distribution of (a) the central brightness m_p^0 of the perinuclear formations and (b) the central brightness m_b of the bars (both in equivalent blue mag arcsec^{-2}) with the length of the bar L_0 (kpc) of the parent galaxies. The straight lines corresponding to $m_p^0 = 23{\cdot}90 - 5 \log L_0$ and $m_b = 23{\cdot}75 - 3 \log L_0$ are shown. The filled squares denote the corrected values for NGC 1672 and 5236. (c) The distribution of the difference $m_b - m_p^0$ with the estimated length of the bar L (kpc) of the bar (see text for details). The value for NGC 5236 denoted by 5236n corresponds to the nucleus before the correction is applied. The corrected value is joined by dotted line. The filled circles represent the classes ϵ and $\epsilon\sigma$, the filled squares σ, and the open circles $\sigma\iota$ and ι. The straight lines $m_b - m_p^0 = k + 2 \log L$ for $k = 1{\cdot}85$, $-0{\cdot}15$, $-0{\cdot}55$ and $-1{\cdot}35$ are shown.

of the disk swept by the bar varies as the square of bar length, the above relation agrees with the mechanism suggested by Sorensen, Matsuda and Fujimoto (1976).

Fig. 10b shows the relationship between the central surface brightness of the bar and the length of the bar. We draw a mean line

$$m_b = 23{\cdot}75 - 3 \log L_0 \text{ (kpc)}$$

with the realistic values of NGC 1672 and 5236. Kalloglyan (1977) and Kormendy (1979) have shown that the mean surface brightness of the bars is nearly constant for all barred galaxies. The above relation would then imply that intensity falls more rapidly in the longer bars than in the shorter ones.

The above two relations are derived from rather scanty data. We support these conclusions from the additional photometric data in Table 2. We plot in Fig. 10c, the difference $m_b - m_p^0$ for 26 galaxies against log L. The relationship

$$m_b - m_p^0 = k + 2 \log L \text{ (kpc)}$$

which conforms with the previous two relations fits the points well with

$k =$ 1·85 for NGC 210 and the nucleus of NGC 5236

$= -$ 0·15 for class σ

$= -$ 0·55 for classes $\epsilon\sigma$ and ϵ

$= -$ 1·35 for classes $\sigma\iota$ and ι.

The difference in the zero points for different classes and the anomalous behaviour of NGC 210 and 5236 are discussed in the following section.

7. Discussion and conclusions

The central regions of Sérsic-Pastoriza galaxies contain bright substructures of two different scale lengths: (a) a nucleus of radius 300–900 pc generally redder than its surroundings and (b) a perinuclear formation of radius 1·3–2·4 kpc. There is a range in which the relative strength of the two components varies. The perinuclear formation is very faint in class κ while the nucleus is very faint in class ι. The classes ϵ, $\epsilon\sigma$ and σ contain both the components. While the perinuclear formation of class σ contains giant complexes of the H II regions, the members of class ϵ do not contain significant amount of ionized gas. The class $\epsilon\sigma$ is intermediate between σ and ϵ while the class $\sigma\iota$ is intermediate between σ and ι.

The parent galaxies of classes ϵ, $\epsilon\sigma$ and σ appear morphologically different from those of classes $\sigma\iota$ and ι. The former group contains more *B* and *AB* spirals (90 per cent against 63) and is more luminous ($\Lambda \sim 0{\cdot}5$ against 1·0) as compared with the latter group. The position of class κ is not very clear because of insufficient statistics on luminosity. The structures of this class appear quite often in SA galaxies too. These remarks suggest that the classes ϵ, $\epsilon\sigma$ and σ belong to a single group of events which differ from the objects of other classes. The burst of star formation giving rise to bright H II regions in class σ may cease eventually and the perinuclear formation may change into the one similar to the class ϵ. The perinuclear formations of classes $\sigma\iota$ and ι are prolate as seen from the scatter in $\log \rho$ —$\log R$ diagram (Fig. 9). Ovoidal and barlike distortions are highly probable even in the classes ϵ, $\epsilon\sigma$ and σ.

Since the bursts of star formation in the central regions of S-P galaxies are of a transient nature, the mechanism for the supply of gas has been an important problem (Wakamatsu and Nishida 1980). Two possible mechanisms are: (a) mass loss from stars in the nuclear region and (b) infall of gas from bar-disk region as suggested by Sorensen, Matsuda and Fujimoto (1976).

The observation that the central brightness of the perinuclear component increases linearly with the square of the bar length (Fig. 10a) supports the mechanism (b). The high specific angular momentum in the perinuclear component also supports this view against the mechanism (a) (Wakamatsu and Nishida 1980). The mechanism (a) may operate in the formation of some nuclei, probably in class κ which occur often in SA galaxies too (NGC 3611, 4212, 4369).

Since the bursts of star formation are transient in nature we should be able to see

different evolutionary stages in different galaxies. An evolution from class σ towards ϵ is very likely as suggested by the lack of H_α emission from class ϵ structures. The brightness of the perinuclear component decreases as the massive stars evolve and die. Thus the $\epsilon\sigma$ and ϵ structures fall below the line for σ in Fig. 10c.

The galaxies with lower luminosity have less gas in the bar-disk region and hence the gas infall would be lower in these cases. Thus $\sigma\iota$ and ι structures result which exhibit the same activity to a much smaller degree (Fig. 10c). Once the gas condenses to the centre, its dynamics may be ruled more by the bar potential than by the disk and halo. Hence, the $\sigma\iota$ and ι structures appear more prolate than the systems of other classes. We have thus been able to separate the activity of differing degree ($\sigma\iota$ and ι) and also in different stages of evolution (from σ towards ϵ). The objects of different classes should be compared with appropriate theoretical models.

The anomalous behaviour of NGC 210 and the nucleus of NGC 5236 in Fig. 10c invites comments. The magnitude difference for NGC 5236n corresponds to the difference between the peak surface brightness of the nucleus and the peak surface brightness of the perinuclear region. Thus it does not belong to the set of values represented in the figure. However, it opens a new question for future investigations, whether the activity in the nucleus is also related to the bar, probably through the perinuclear formation. NGC 210 contains, on the other hand, a well defined perinuclear component typical of class ϵ. It is the brightest, and one of the largest perinuclear formations in our sample. Unfortunately, it is not a well studied galaxy. Detailed surface photometry of NGC 210 and radio observations on its H I content and its environment will help to clarify the situation. This galaxy merits being on the search list for compact IR, X-ray and radio nucleus.

An important off-shoot of the present investigations is the dependence of the central surface brightness of the bar on the size of the bar. The central surface brightness of the bar increases directly with the bar length with an exponent close to unity. Incorporating the observations of Kalloglyan (1977) and Kormendy (1979) that the mean surface brightness of the bars is constant for all barred galaxies, we conclude the surface brightness of the larger bars falls steeper than that of the shorter ones.

Acknowledgements

The material presented in this paper constitutes a major part of the doctoral thesis submitted to the Madurai Kamaraj University. It is indeed a great pleasure to express my deep gratitude to Dr M. K. V. Bappu, my thesis supervisor, for impressing upon me the importance of Sérsic's list, for the design of the instrumentation used in this investigation at the Kavalur Observatory, and for constant encouragement. Thanks are also due to several friends and colleagues at the Indian Institute of Astrophysics whose assistance has been invaluable and was readily available at the crucial moments.

References

Alcaino, G. 1976, *Astr. Astrophys. Suppl. Ser.*, **26**, 261.
Alloin, D., Kunth, D. 1979, *Astr. Astrophys.*, **71**, 335.

Benedict, G. F. 1980, *Astr. J.*, **85**, 513.
Burbidge, E. M. 1962, in *The Distribution and Motion of Interstellar Matter in Galaxies*, Ed. L. Woltjer, W. A. Benjamin, Inc., New York, p. 123.
Burbidge, E. M., Burbidge, G. R. 1960, *Astrophys. J.*, **132**, 30.
Burbidge, E. M., Burbidge, G. R. 1968, *Astrophys. J.*, **151**, 99.
de Vaucouleurs, G. 1977, in *IAU Coll. 37: L'Evolution des Galaxies et ses implications cosmologiques*, CNRS, p. 301.
de Vaucouleurs, G., de Vaucouleurs, A. 1961, *Mem. R. astr. Soc.*, **68**, 69.
de Vaucouleurs, G., de Vaucouleurs, A., Corwin, H. G. 1976, *Second Reference Catalogue of Bright Galaxies*, University of Texas Press, Austin.
Geyer, E. H. 1978, in *Modern Techniques in Astronomical Photography*, Eds R. M. West and J. L. Heudier, European Southern Observatory, Geneva, p. 297.
Glass, I. S. 1976, *Mon. Not. R. astr. Soc.*, **175**, 191.
Griffiths, R. E., Feigelson, E., van Speybroeck, L. 1979, *Bull. Am. astr. Soc.*, **11**, 466.
Kalloglyan, A. T. 1971, *Astrophys.*, **7**, 109.
Kelton, P. W. 1980, *Astr. J.*, **85**, 89.
Kleinmann, D. E., Low, F. J. 1970, *Astrophys. J.*, **161**, L203.
Kleinmann, D. E., Wright, E. L. 1974, *Astrophys. J.*, **191**, L19.
Kormendy, J. 1979, *Astrophys. J.*, **227**, 714.
Kormendy, J. 1980, in *Two Dimensional Photometry*, Eds P. Crane and K. Kjar, European Southern Observatory, Geneva, p. 191.
Ku, W. H.-M., Chanan, G. A., Helfand, D. J., Long, K. S. 1979, *Bull. Am. astr. Soc.*, **11**, 466.
Morgan, W. W. 1958, *Publ. astr. Soc. Pacific*, **70**, 364.
Morgan, W. W., Walborn, N. R., Tapscott, J. W. 1971, in *Nuclei of Galaxies*, Ed. D. J. K. O'Connell North Holland Pub. Co., Amsterdam, p. 27.
Oka, S., Wakamatsu, K., Sakka, K., Nishida, M., Jugaku, J. 1974, *Publ. astr. Soc. Japan*, **26**, 289.
Osmer, P. S., Smith, M. G., Weedman, D. W. 1974, *Astrophys. J.*, **192**, 279.
Pastoriza, M. G. 1975, *Astrophys. Sp. Sci.*, **33**, 173.
Prabhu, T. P. 1978, *Kodaikanal Obs. Bull. Ser. A*, **2**, 105.
Prabhu, T. P. 1979, *PhD thesis*, Madurai Kamaraj University.
Prabhu, T. P. 1980, *Astrophys. Sp. Sci.*, **68**, 519.
Rieke, G. H., Lebofsky, M. J. 1978, *Astrophys. J.*, **220**, L38.
Rieke, G. H., Low, F. J. 1972, *Astrophys. J.*, **176**, L95.
Sandage, A. 1978, *Astr. J.*, **83**, 904.
Sérsic, J. L. 1968, *Atlas de Galaxies Australes*, Observatorio Astronomico, Cordoba.
Sérsic, J. L. 1973, *Publ. astr. Soc. Pacific*, **85**, 103.
Sérsic, J. L., Pastoriza, M. G., 1965, *Publ. astr. Soc. Pacific*, **77**, 287.
Sorensen, S. A., Matsuda, T., Fujimoto, M. 1976, *Astrophys. Sp. Sci.*, **43**, 491.
Talbot, R. J., Jensen, E. B., Dufour, R. J. 1979, *Astrophys. J.*, **229**, 91.
Telesco, C. M., Harper, D. A. 1980, *Astrophys. J.*, **235**, 392.
Turnrose, B. E. 1976, *Astrophys. J.*, **210**, 33.
van der Kruit, P. C. 1973, *Astr. Astrophys.*, **29**, 231.
Véron, M. P., Véron, P., Zuiderwijk, E. J. 1980, *ESO Scientific Preprint*, No. 109.
Véron, P., Lindblad, P. O., Zuiderwijk, E. J., Véron, M. P., Adam, G. 1979, *Astr. Astrophys.*, **87**, 245.
Véron, P., Véron, M. P., Bergeron, J., Zuiderwijk, E. J. 1980, *ESO Scientific Preprint* No. 83.
Wakamatsu, K., Nishida, M. T. 1980, *Publ. astr. Soc. Japan*, (in press).
Ward, M. J., Wilson, A. S., Disney, M. J., Elvis, M., Maccacaro, T. 1978, *Astrophys. J.*, **223**, 788.